Supporting Information

Structural Flexibilities and Gas Adsorption Properties of One-Dimensional Copper(II) Polymers with Paddle-Wheel Units by Modification of Benzoate Ligands

Kiyonori Takahashi,[†] *Norihisa Hoshino,*[†, ‡] *Takashi Takeda,*[†, ‡] *Shin-ichiro Noro,*[¶] *Takayoshi Nakamura,*[¶] *Sadamu Takeda,*[±] *Tomoyuki Akutagawa* *[†, ‡]

[†] Graduate School of Engineering, Tohoku University, Sendai 980-8579, Japan.

[‡] Institute of Multidisciplinary Research for Advanced Materials (IMRAM), Tohoku University, 2-1-1 Katahira, Aoba-ku, Sendai 980-8577, Japan.

[±] Graduate School of Science, Hokkaido University, Sapporo 060-0810, Japan.

[¶] Research Institute for Electronic Science, Hokkaido University, Sapporo 001-0020, Japan.

Infrared spectroscopy

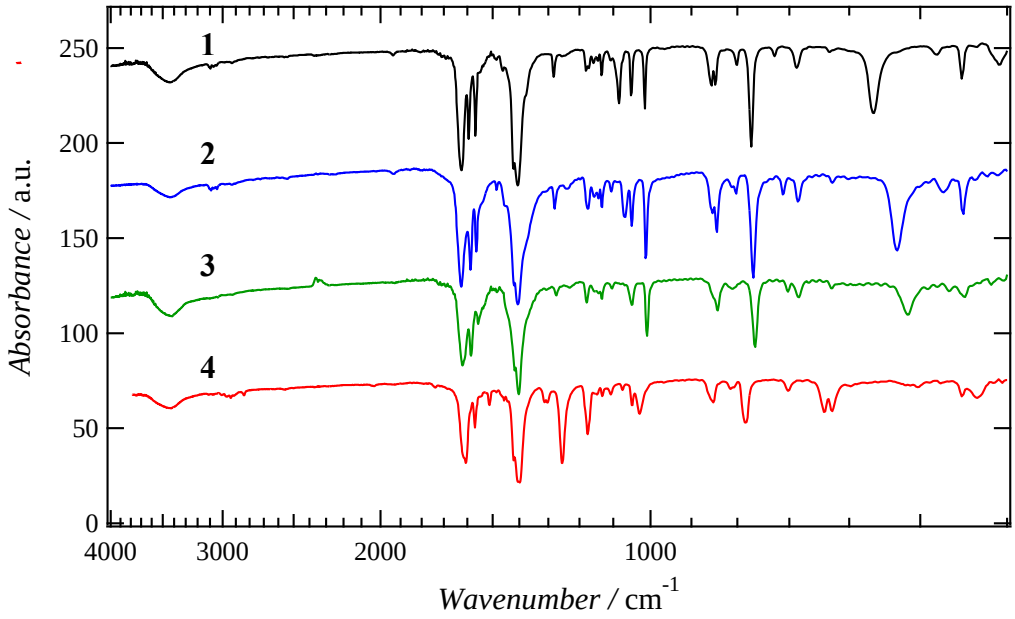

Figure S1. Infrared Spectra of **1** ~ **4**, ranged from 700 to 4000 cm^{-1}. Black, blue, green and red colored lines correspond with **1**, **2**, **3** and **4**, respectively.

Powder X-ray Diffraction Patterns

To determine structures of the single crystal and powder samples were same, Powder X-ray radiation diffraction spectra of powder samples were measured and compared with patterns simulated from single crystal X-ray structural analyses.

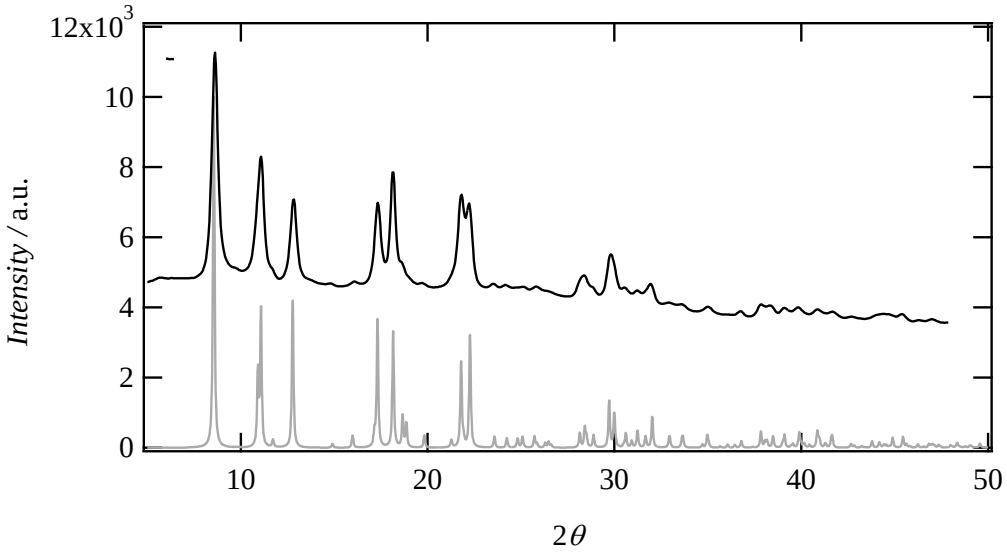

Figure S2. The powder X-ray diffraction patterns for **1**. The black-colored pattern was measured at 100 K. The gray-colored pattern was simulated from the single crystal structure of **1**.

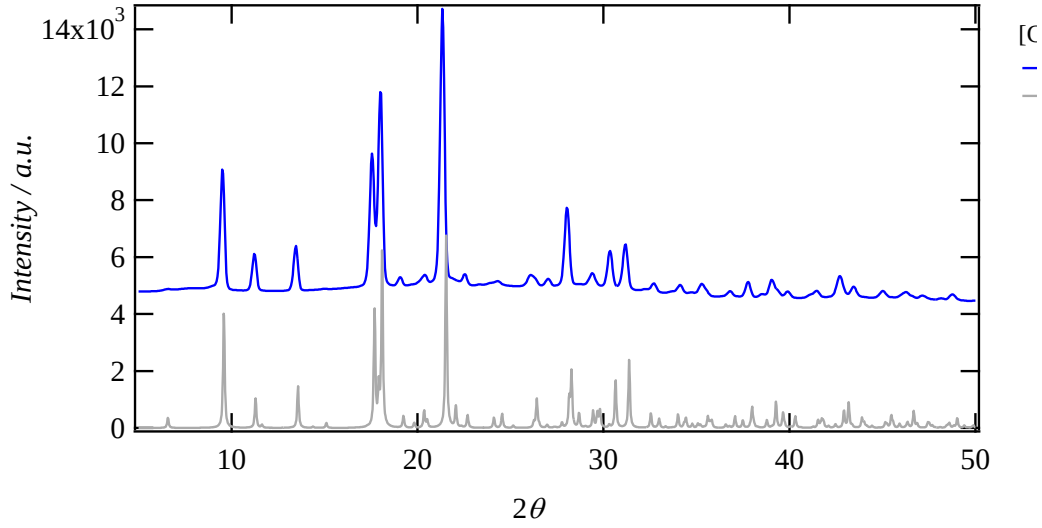

Figure S3. The powder X-ray diffraction patterns for **2**. The blue-colored pattern was measured at 100 K. The gray-colored pattern was simulated from the single crystal structure of **2**.

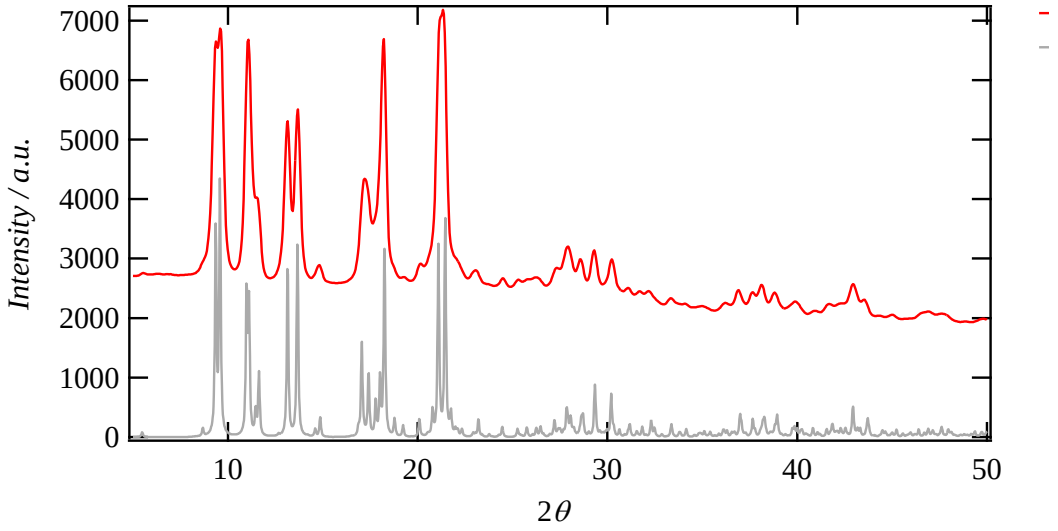

Figure S4. The powder X-ray diffraction patterns for **4**. The black-colored pattern was measured at 100 K. The gray-colored pattern was simulated from the single crystal structure of **4**.

Figures S2 ~ S4 summarized the powder patterns of crystal **1**, **2** and **4**. To determine the structures of crystalline powder samples and single crystal structures obtained from another synthesized methods were the same, the powder X-ray diffraction patterns were measured. The figures showed good agreement with each patterns. Therefore the crystalline powder samples had the same structures mentioned in this paper.

Thermogravimetry analysis (TG).

TG analyses were carried out using a Rigaku Thermo plus TG8120 thermal analysis station using an Al_2O_3 reference in the temperature range from 300 to 600 K with a heating rate of 5 K min-1 under Ar.

Although over 20% weight-losses were observed over 500 K (**1**), 520 K(**2**), 450 K (**3**), 400 K(**4**) in TG diagrams, these were not corresponded to weight-loss of crystallization solvents because of the absence of crystallization solvents in the crystal structures.

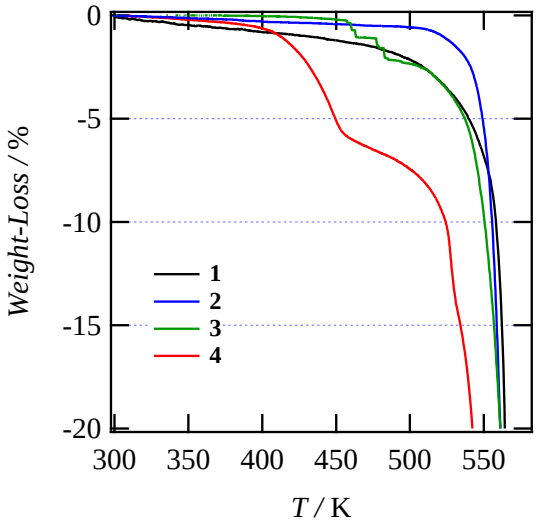

Figure S5. TG diagram of crystals **1**, **2**, **3**, and **4** under argon flow.

Thermogravimetry- differential scanning calorimetry (DSC) measurements.

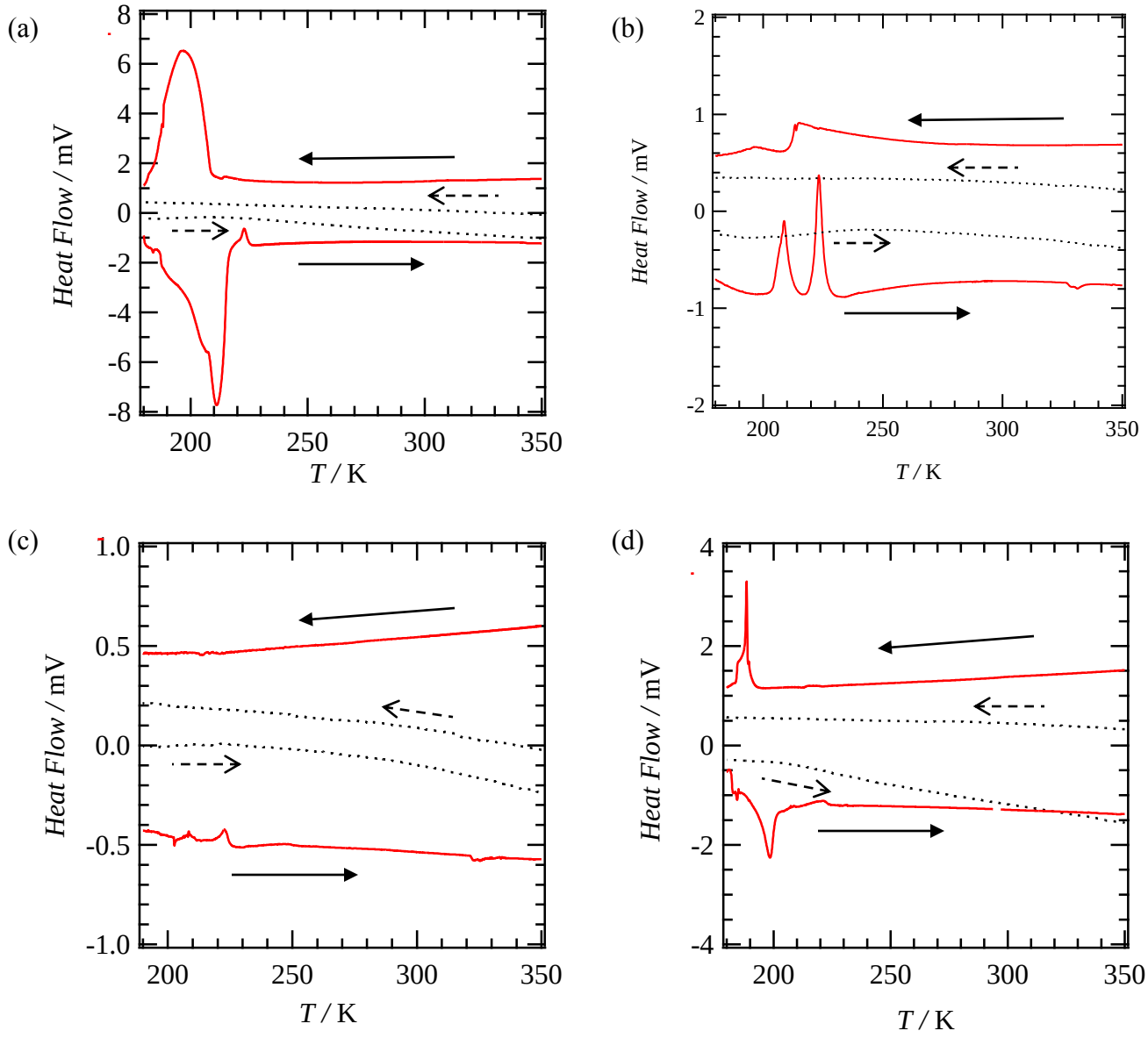

Figure S6. DSC traces for (a) crystals **1**, (b) **2**, (c) **3** and (d) **4** under Air (dotted line) and CO_2 gas flow (red line) with a scan rate of 5 K min^{-1}. Right- and left-pointing allows mean heating and cooling processes near the measured values and solid and dotted lines mean the scan under the CO_2 condition and Air.

The DSC analyses under the CO_2 condition were carried out using Mettler Toledo DSC 1 STARe System using an Al_2O_3 reference in the temperature range from 170 to 350 K. The scan rate and CO_2 flow rate were 5 K min^{-1} and 60 mL min^{-1}, respectively. DSC analyses under Air were conducted using a Rigaku Thermo plus DSC 8230 with Al_2O_3 as a reference in the temperature range from 170 to 350 K. The scan rate was 5 K min^{-1}.

Crystal shapes

(a) 

(b) 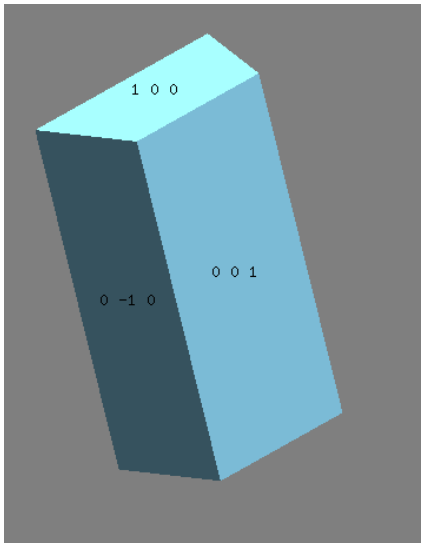

Figure S7. (a) Crystal shape of **2** mounted on thin polyimide films (MiTeGen MicroMounts). (b) Crystal shape calculated by Rigaku RAPID-II.

The pictures of crystal shape of **2** and **3** were taken and crystal shapes of them were calculated for Numerical Absorption Correction method. The shapes of these crystals were like block. The shapes of crystal **1** and **4** were similar to them.

(a)

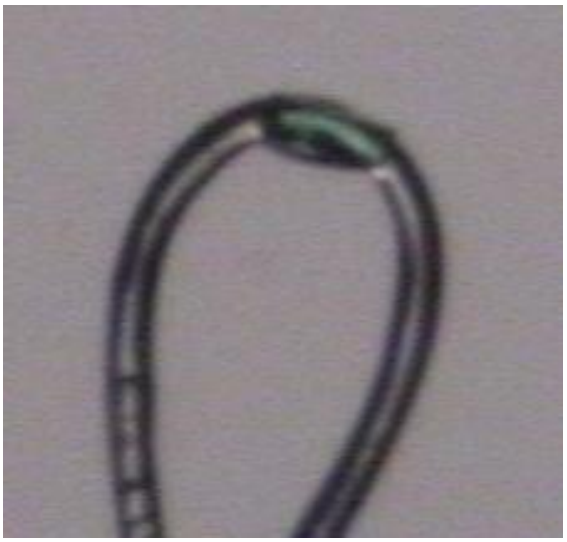

(b)

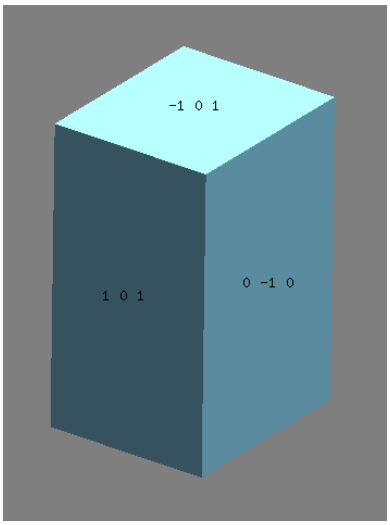

Figure S8. (a) Crystal shape of **3** mounted on thin polyimide films (MiTeGen MicroMounts). (b) Crystal shape calculated by Rigaku RAPID-II.

Crystal Structures

Independent structures and coordination geometries**.**

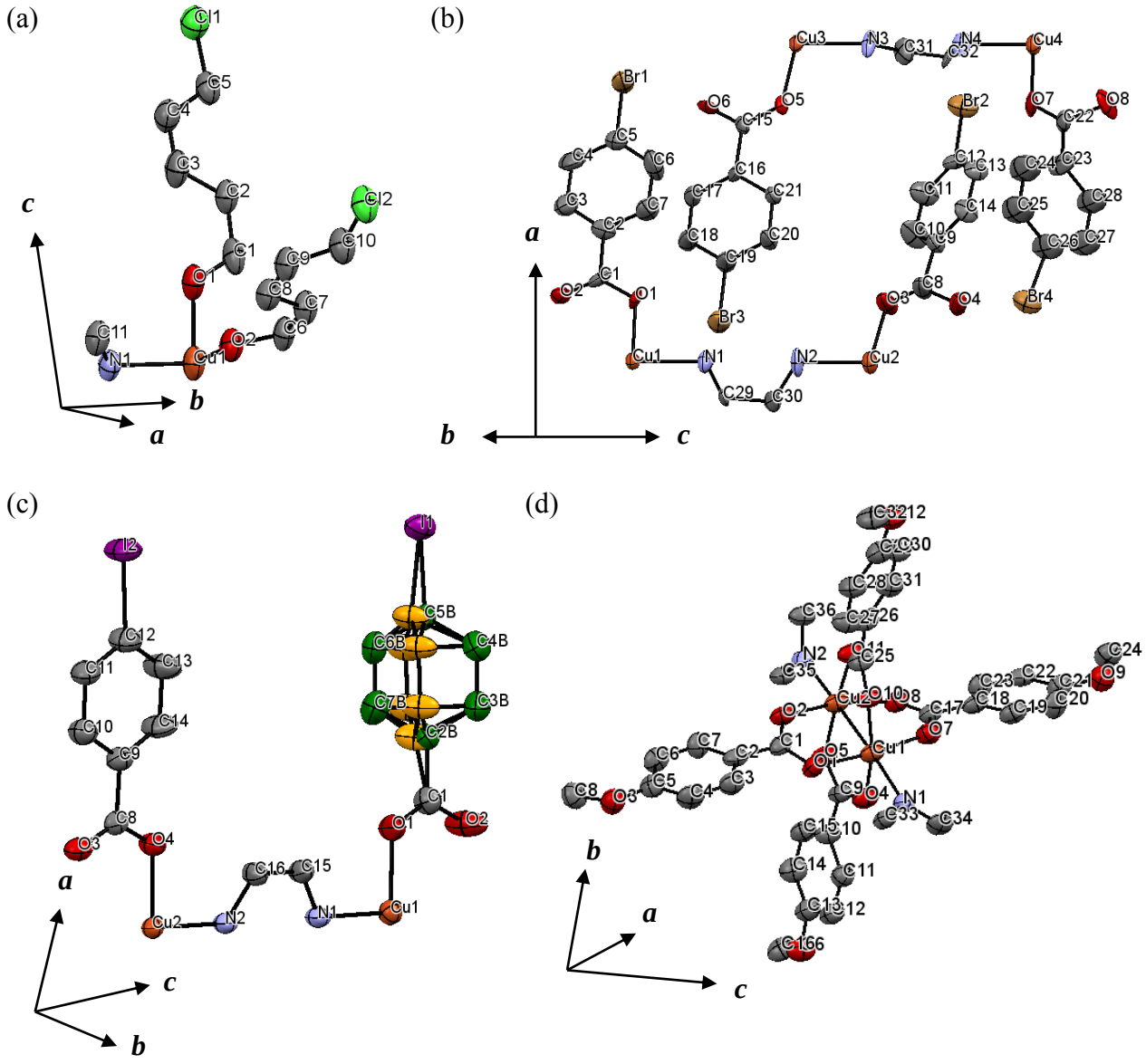

Figure S9. Independent structures and atom numbers of (a) **1**, (b) **2**, (c) **3** and (d) **4**. The disordered sites of crystal **3** were highlighted with orange (Ring 3B) and green (Ring 3C) colors.

The crystallographic independent structures of **1**, **2**, **3** and **4** were shown in Figures S8. Inversion center of crystal **1** was between two coppers in paddle-wheel unit. .

Table S1. The Torsion angles of selected atoms in crystals **1 - 4**.

	around O-C-benzoate		around benzoate-methoxy group	
	selected atoms	Torsion angle, deg	selected atoms	Torsion angle, deg
1A	O1-C1-C2-C3	0.64		
1B	O2-C5-C7-C8	-2.88		
2A	O1-C1-C2-C7	-0.24		
2B	O3-C8-C9-C10	-42.67		
2C	O5-C15-C16-C21	-3.93		
2D	O7-C22-C23-C24	-34.12		
3A	O1-C1-C2A-C7A	65.45		
3B	O1-C1-C2B-C7B	-47.93		
3C	O4-C8-C9-C14	3.45		
4A	O1-C1-C2-C3	14.18	C6-C5-O3-C8	9.88
4B	O4-C9-C10-C11	3.00	C14-C13-O6-C16	7.52
4C	O8-17-C18-C19	-5.09	C14-C13-O6-C16	7.25
4D	C10-C25-C26-C27	-45.2	C14-C13-O6-C16	2.92

Table S1. summarizes the torsion angles of selected atoms in crystal 1 – 4. Torsion angles were calculated by Mercury Version 3.3

Packing Structures

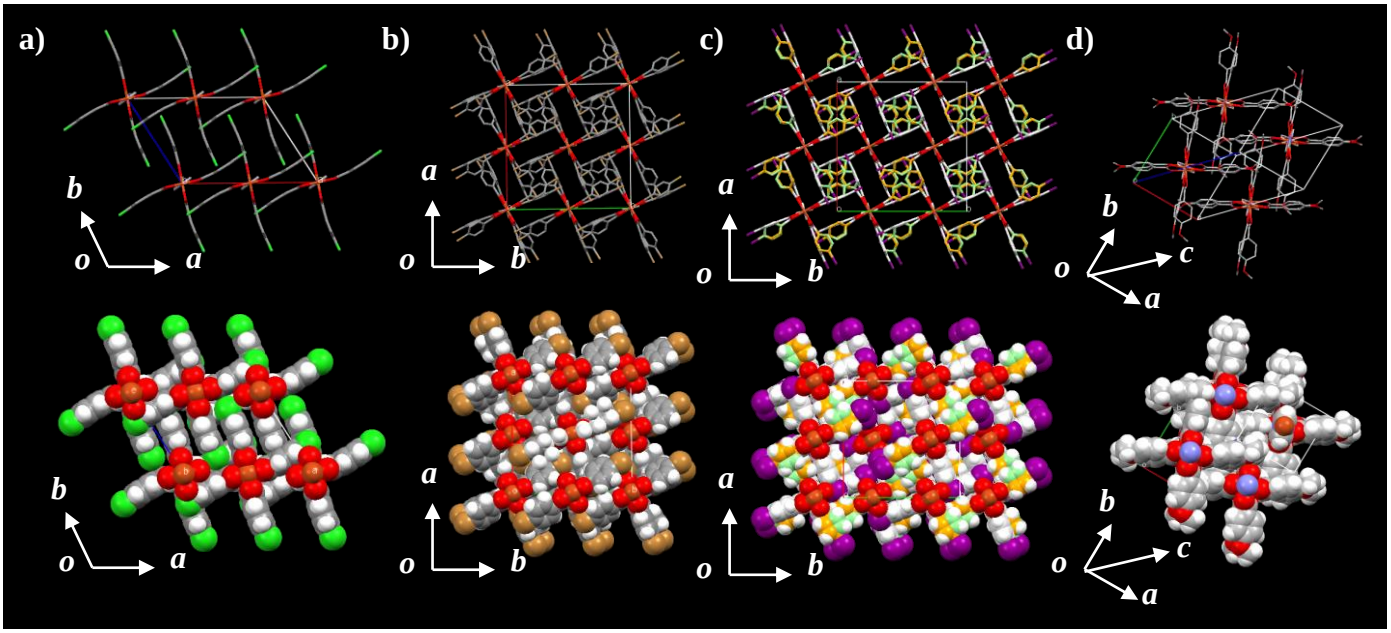

Figure S10. Packing structures for a) **1**, b) **2**, c) **3** and d) **4**. Upper figures were modeled by ball and stick, lower figures were modeled by CPK.

From the packing structures, crystallization solvents and effective void space were not found.

Intermolecular Interactions

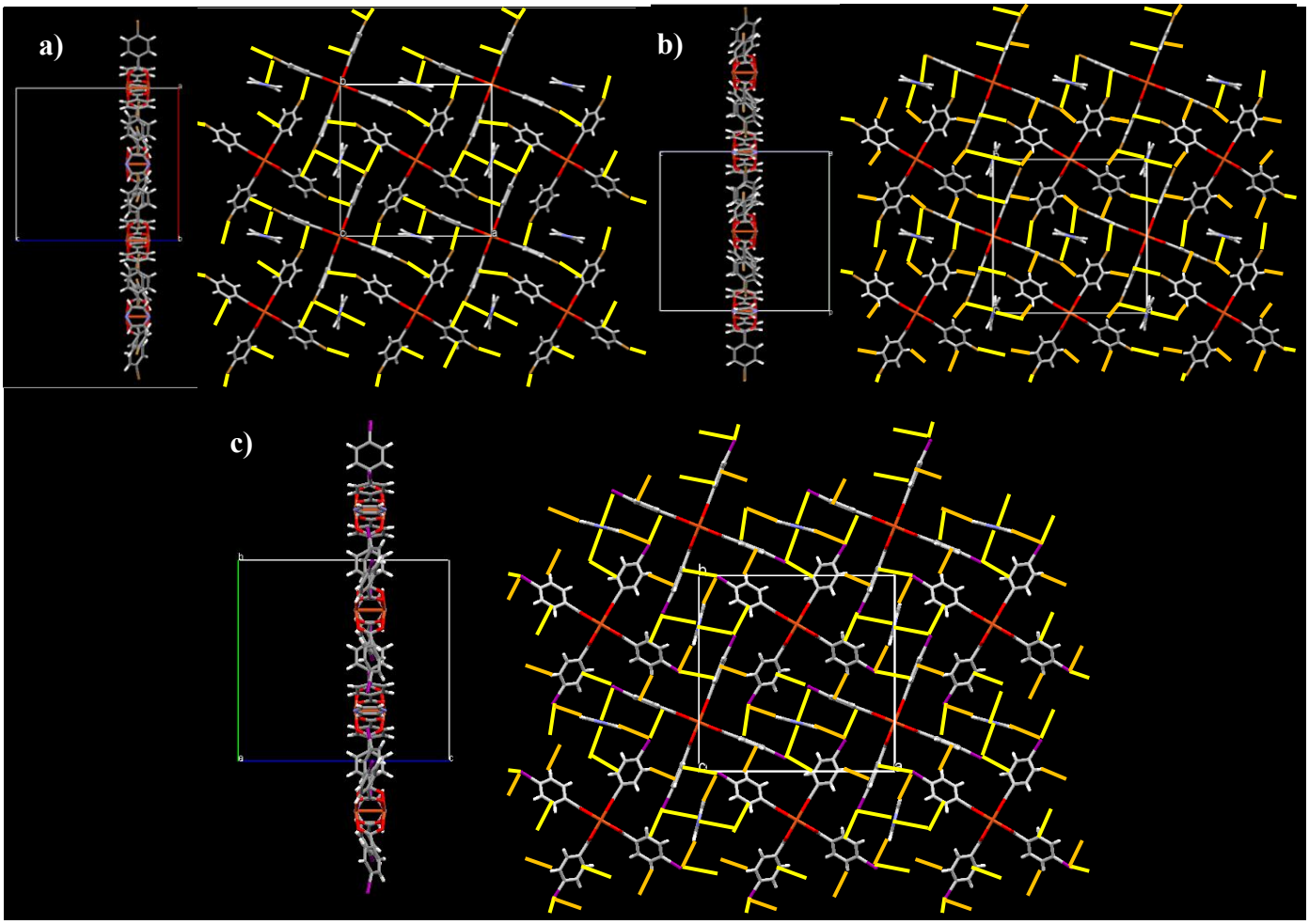

Figure S11. Two dimensional layered interactions for a) crystal **2**, where all *p*-BrBA ligands were consistent with **2A** and **2B**, b) crystal **2**, where *p*-BrBA ligands were consistent with **2**C and **2D**, and c) crystal **3**. Left figures in each were viewed along *a* axis, which were corresponded to right figures. In these figures yellow and orange lines were corresponded to halogen•••H and halogen•••π interactions, respectively. All lines were corresponded to the distances less than the sum of vdW radii of two corresponded atoms.

Offset Face-to-Face π•••π Stacking.

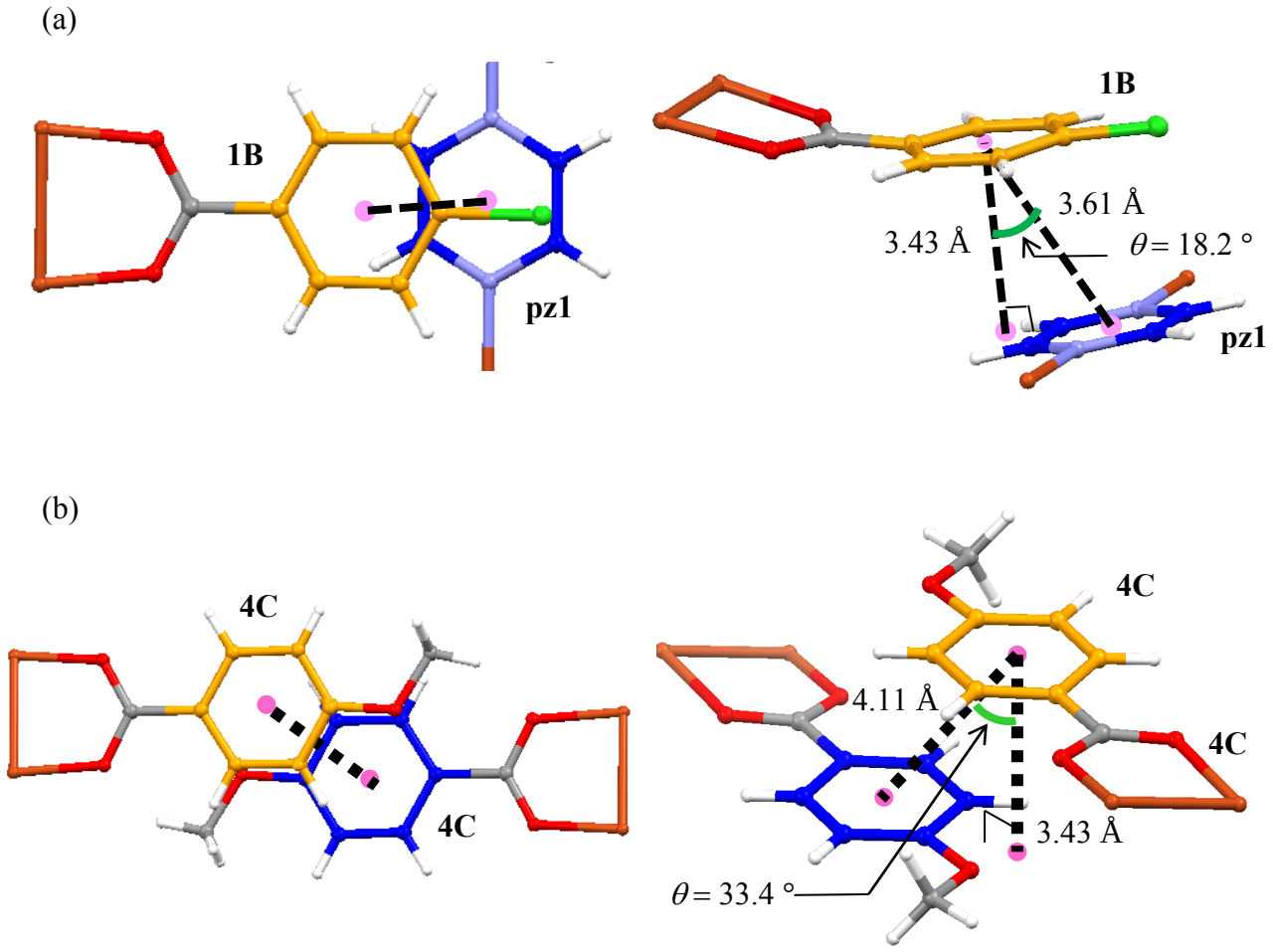

Figure S12. Offset π•••π stacking viewed along top-down (Left) and side direction (Right) between (a) **1B** and **pz1** (crystal **1**), and between **4C** and **4C** (Crystal **4**). The length was picked from the crystal structures and the angles were calculated from the length.

Weak π•••π stacking were observed in the crystals **1** and **4**. This stacking mode was offset face-to-face π•••π. Overlap of π planes between **1B** and **pz1** was larger than that between two **4C**s because of the comparison with the distance between centers of π planes the angles expressed on Figure S12.

Hirshfeld Surface Analyses.

Because the crystal structures of **2** have four independent *p*-BrBA ligand and crystal **3** have disordered sites (named **3B** and **3B'**), each was separated and the site occupancies of their atoms were changed to 1.0 for all Hirshfeld surface analysis.

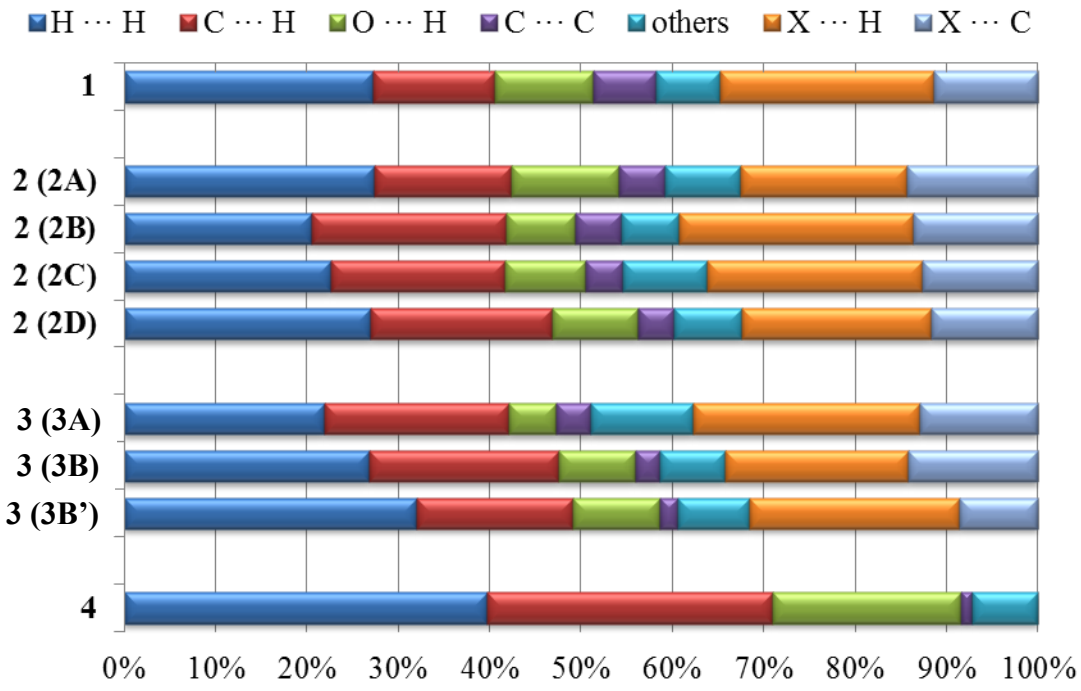

Figure S13. Histograms of the type of nearest neighboring atomic contacts from the 2D fingerprint plots. The average percentages for crystals **2** and **3** in Figure 7 were calculated by these values.

Fingerprint Plot with no fingerprint filtering.

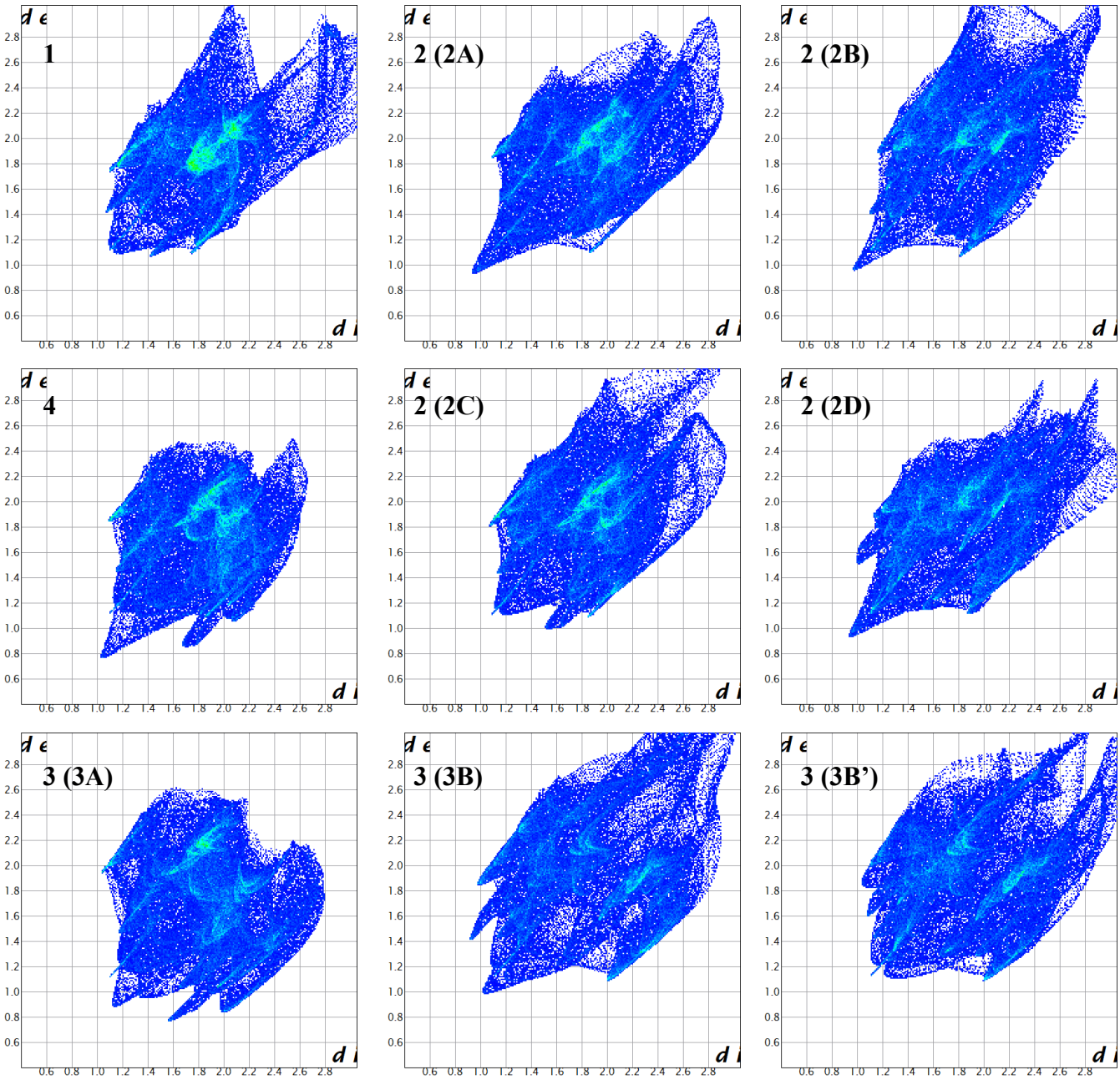

Figure S14. Fingerprint plots of **1** ~ **4**.

Fingerprint Plot with fingerprint filtering highlighting close contacts from H···H.

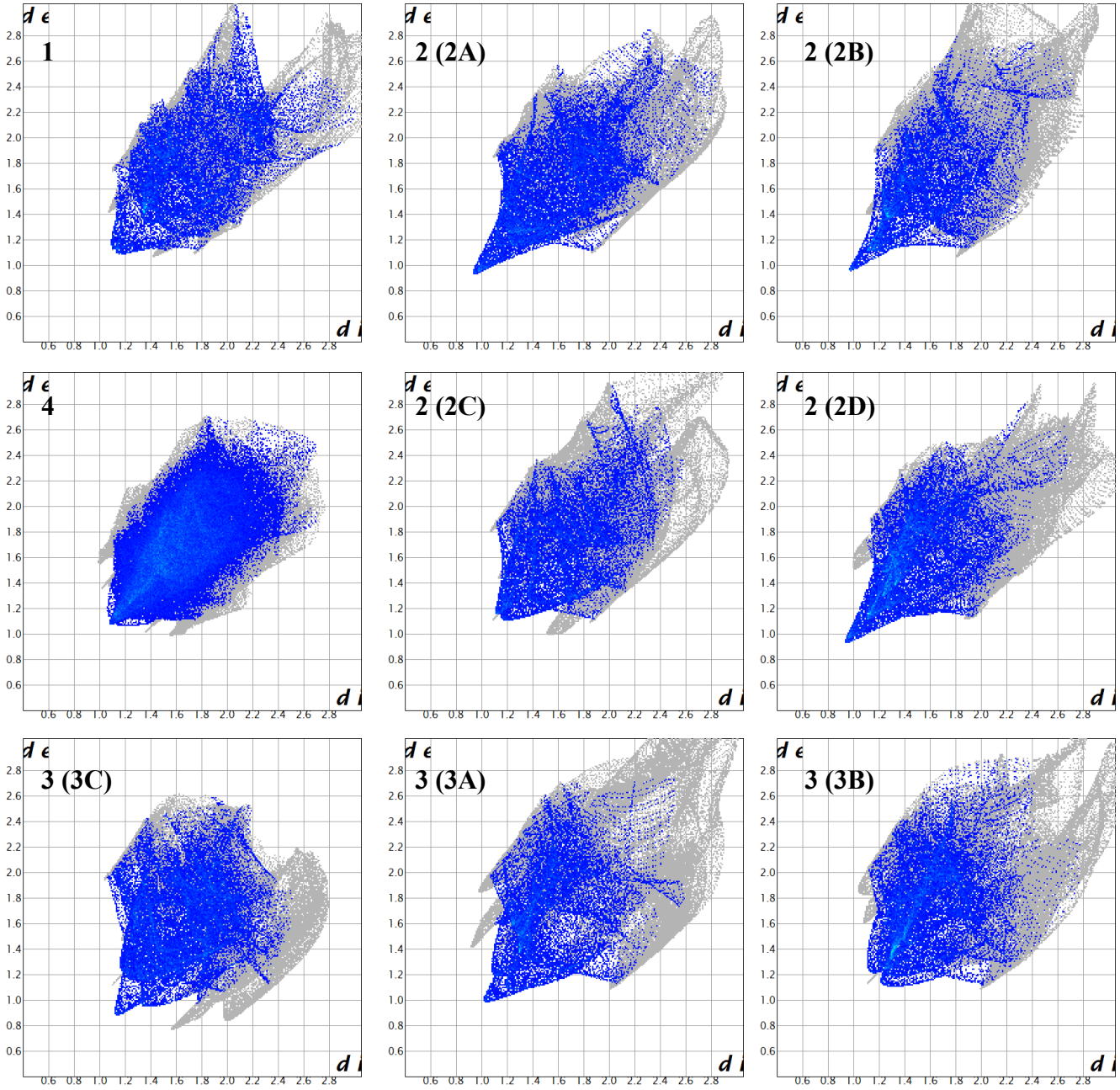

Figure S15. 2D fingerprint plots of H•••H contacts (blue-colored area) along with the other kinds (gray-colored area). The symbols on the upper left side of each plot corresponded to the numbers of crystals and ligands.

Fingerprint Plot with fingerprint filtering highlighting close contacts from C···H.

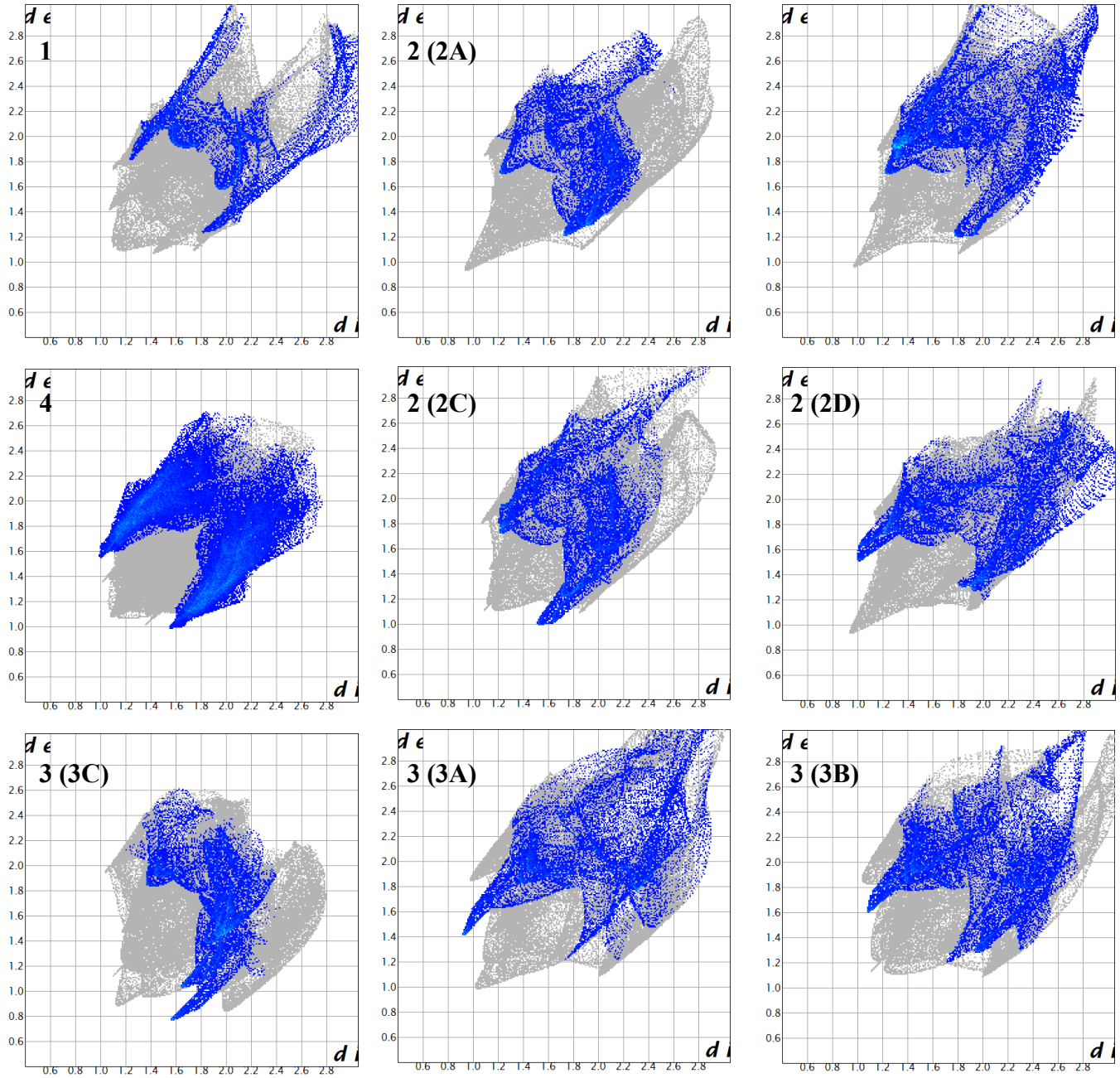

Figure S16. 2D fingerprint plots of C•••H contacts (blue-colored area) along with the other kinds (gray-colored area). The symbols on the upper left side of each plot corresponded to the numbers of crystals and ligands.

Fingerprint Plot with fingerprint filtering highlighting close contacts from O···H.

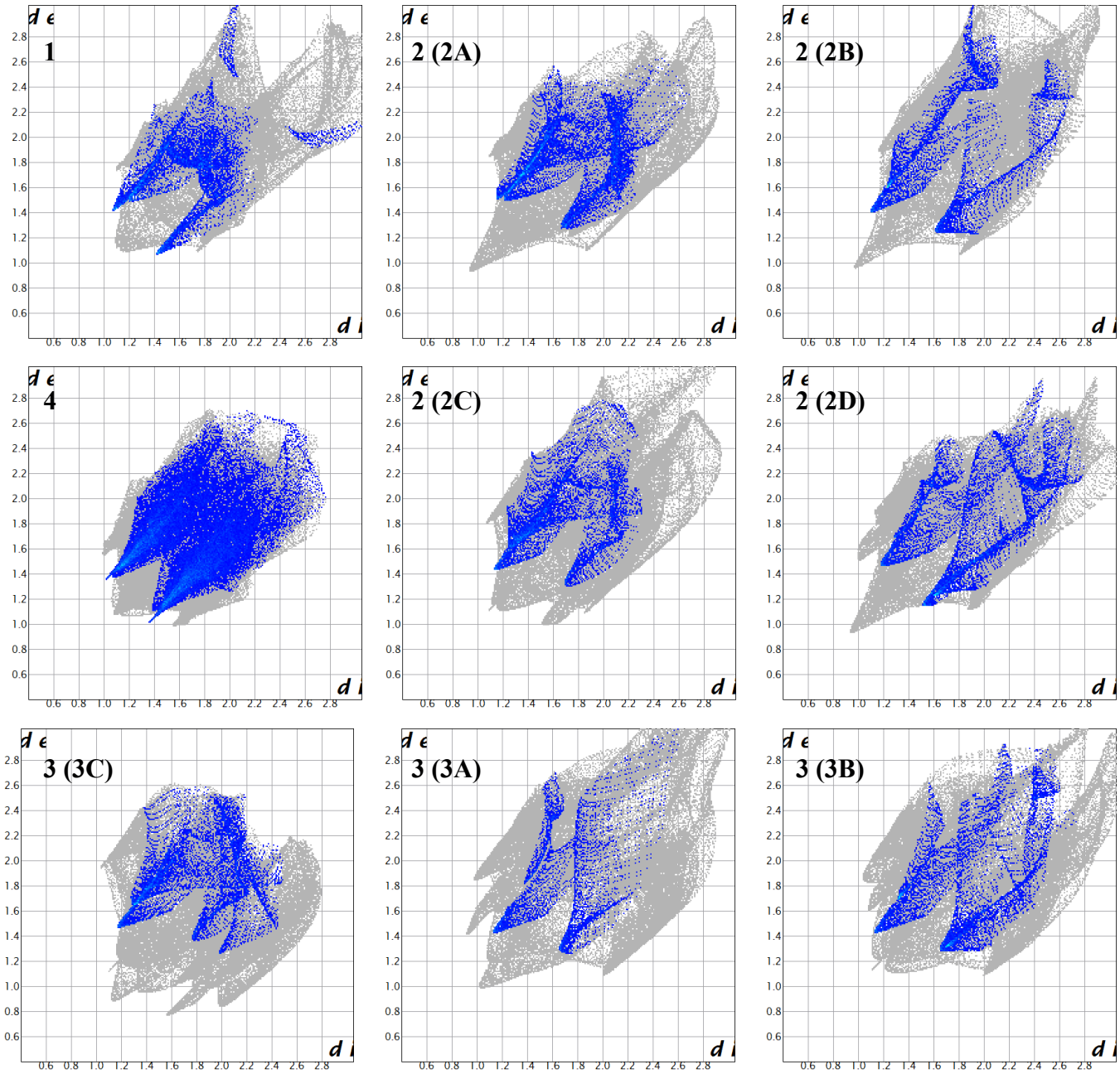

Figure S17. 2D fingerprint plots of O•••H contacts (blue-colored area) along with the other kinds (gray-colored area). The symbols on the upper left side of each plot corresponded to the numbers of crystals and ligands.

Fingerprint Plot with fingerprint filtering highlighting close contacts from halogen···H.

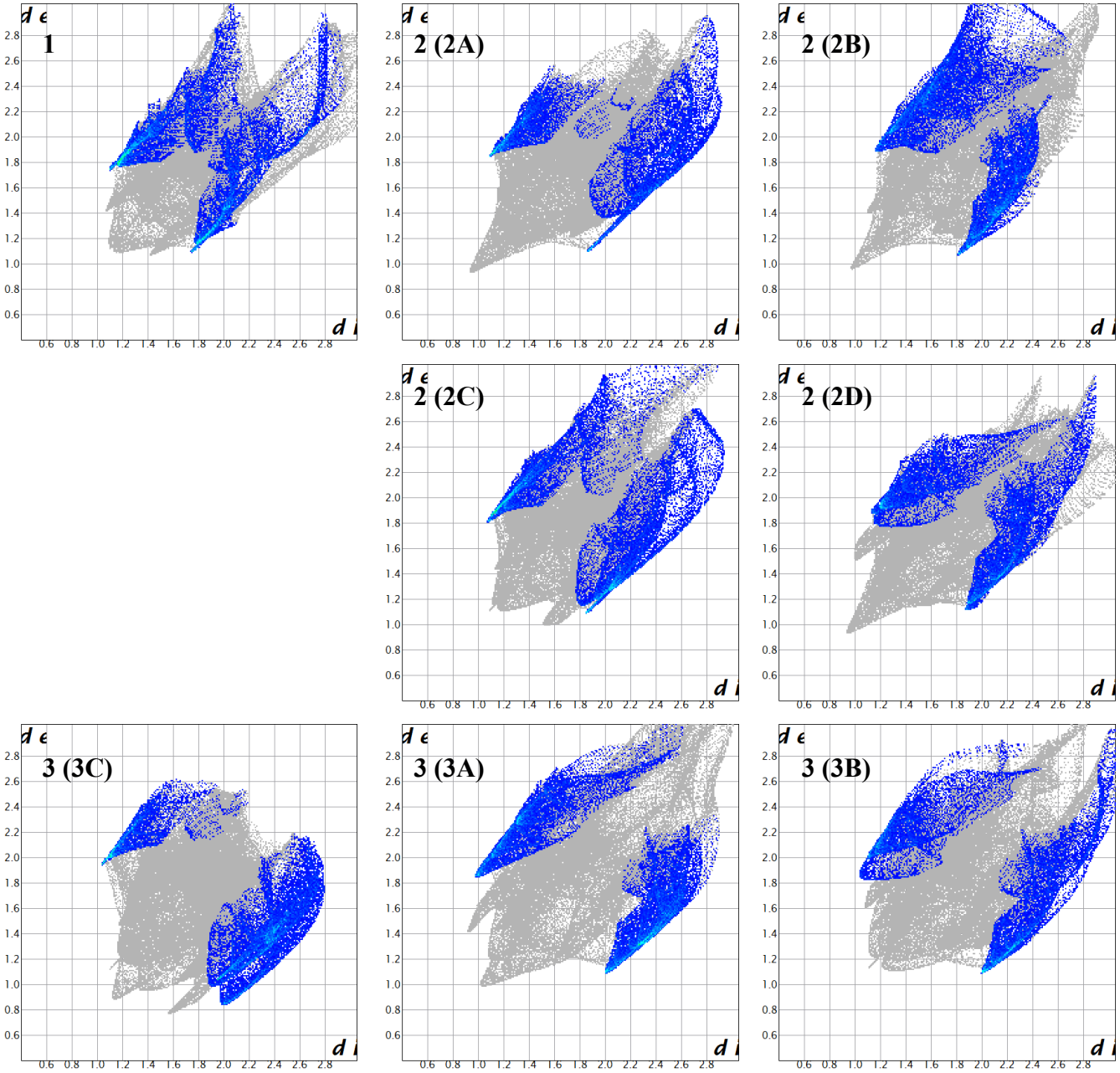

Figure S18. 2D fingerprint plots of halogen•••H contacts (blue-colored area) along with the other kinds (gray-colored area). The symbols on the upper left side of each plot corresponded to the numbers of crystals and ligands.

Fingerprint Plot with fingerprint filtering highlighting close contacts from halogen⋯C.

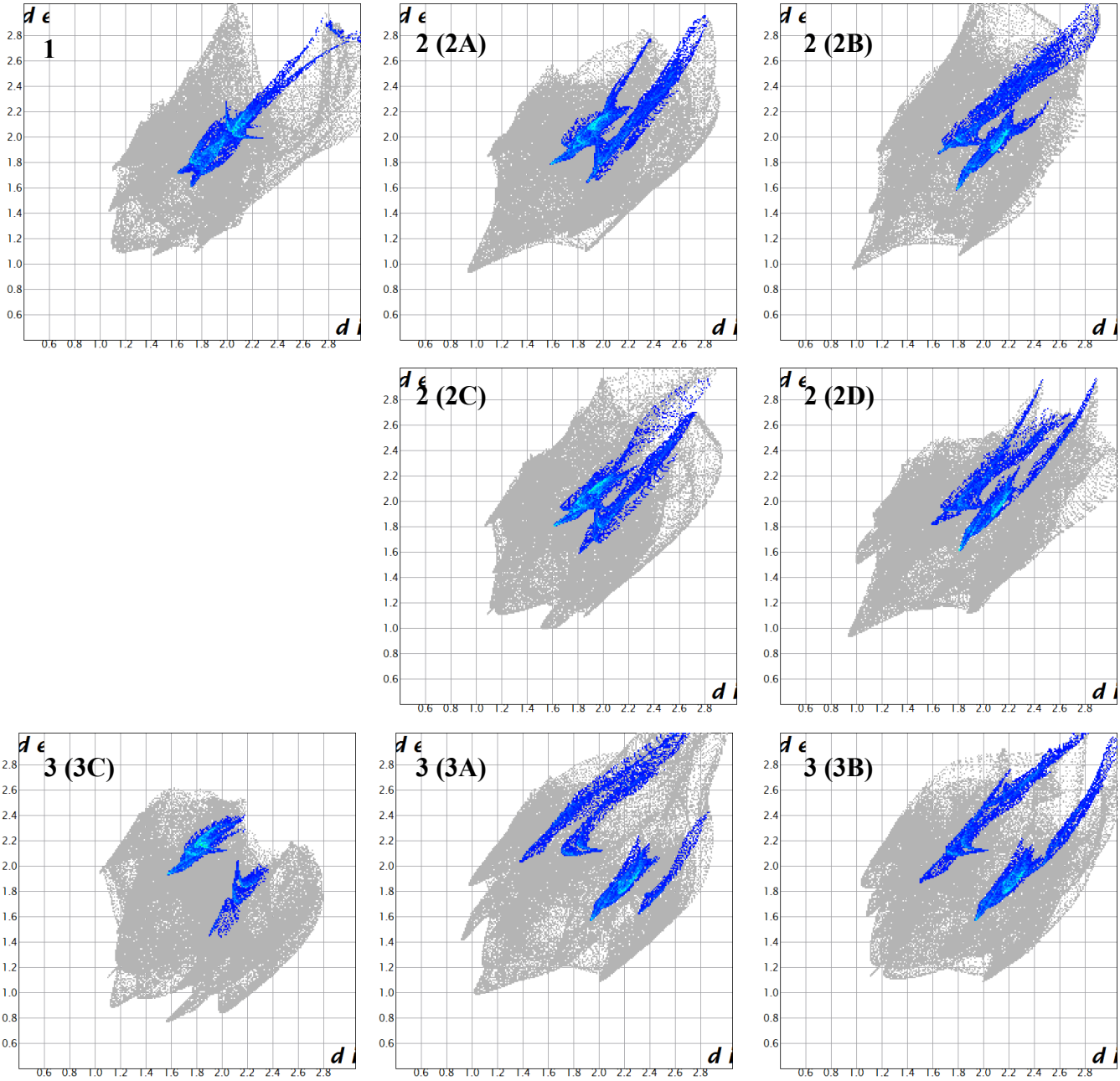

Figure S19. 2D fingerprint plots of halogen•••C contacts (blue-colored area) along with the other kinds (gray-colored area). The symbols on the upper left side of each plot corresponded to the numbers of crystals and ligands.

Curvedness Fit

To evaluate planarity of *p*-XBA ligands related to π•••π interaction for crystal **1** and **4**, curvedness fit were calculated in Hirshfeld Surface analysis.

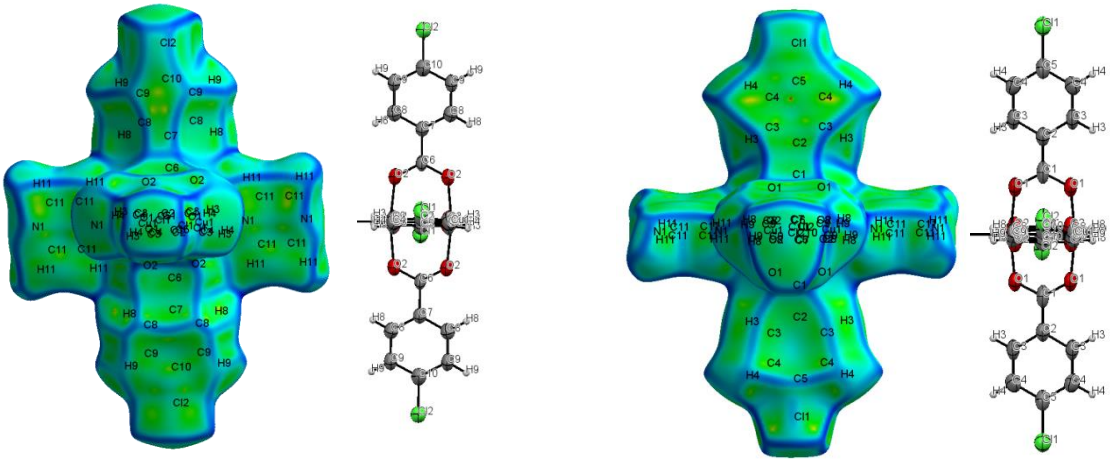

Figure S20. Curvedness fit on **4A** and corresponded atom geometries.

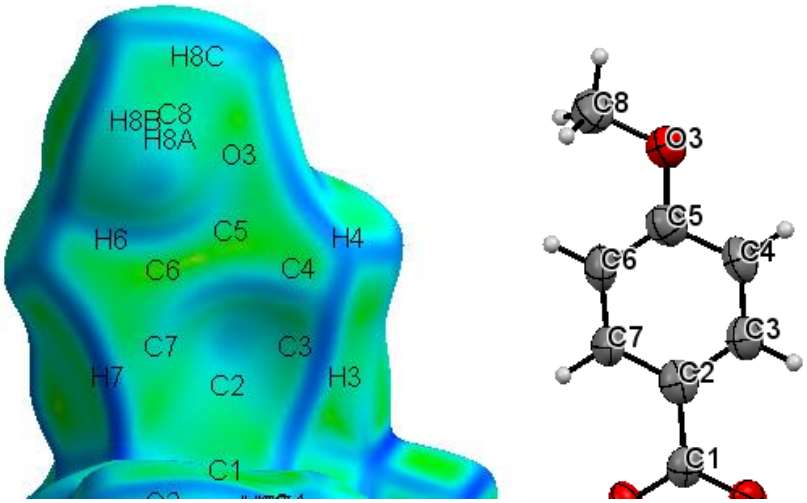

Figure S21. Curvedness fit on **4A** and corresponded atom geometries.

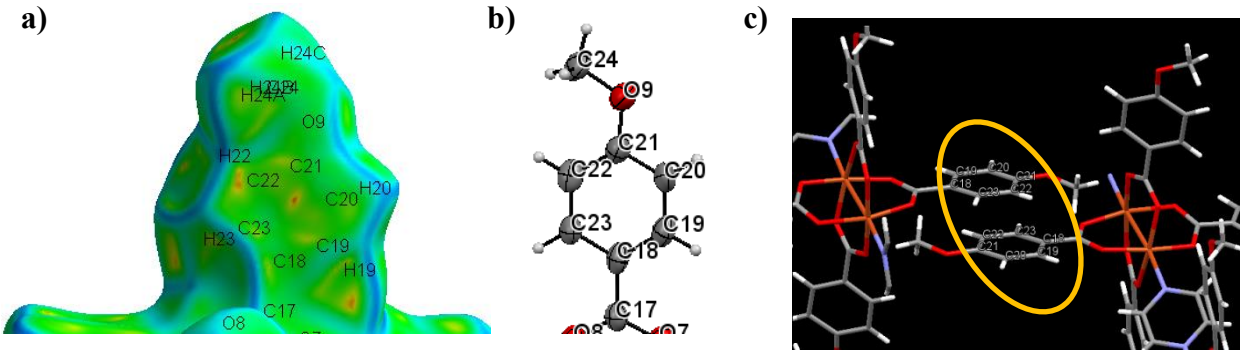

Figure S22. a) Curvedness fit on **4C**, b) corresponded atom geometries of **4C** and c) π•••π interaction between two **4C**.

From the Hirshfeld surface analysis on crystal **1**, Curvedness fit revealed that one plane of **1A** and **pz1** were almost flat. It is corresponded to the existence of π•••π interaction in crystal **1**. By using Curvedness fit for crystal **4**, π•••π interactive planes were also clearly observed.